

# Ultrafast carrier dynamics in single-walled carbon nanotubes probed by femtosecond spectroscopy

Ying-Zhong Ma, Jens Stenger, and Jörg Zimmermann

*Department of Chemistry, University of California, Berkeley and Physical Biosciences Division, Lawrence Berkeley National Laboratory, Berkeley, California 94720-1460*

Sergei M. Bachilo

*Department of Chemistry, Center for Nanoscale Science and Technology, and Center for Biological and Environmental Nanotechnology, Rice University, Houston, Texas 77005*

Richard E. Smalley

*Department of Chemistry, Center for Nanoscale Science and Technology, and Center for Biological and Environmental Nanotechnology, Rice University, Houston, Texas 77005 and Department of Physics, Rice University, Houston, Texas 77005*

R. Bruce Weisman

*Department of Chemistry, Center for Nanoscale Science and Technology, and Center for Biological and Environmental Nanotechnology, Rice University, Houston, Texas 77005*

Graham R. Fleming<sup>a)</sup>

*Department of Chemistry, University of California, Berkeley and Physical Biosciences Division, Lawrence Berkeley National Laboratory, Berkeley, California 94720-1460*

(Received 19 September 2003; accepted 17 November 2003)

Ultrafast carrier dynamics in individual semiconducting single-walled carbon nanotubes was studied by femtosecond transient absorption and fluorescence measurements. After photoexcitation of the second van Hove singularity of a specific tube structure, the relaxation of electrons and holes to the fundamental band edge occurs to within 100 fs. The fluorescence decay from this band is dependent on the excitation density and can be rationalized by exciton annihilation theory. In contrast to fluorescence, the transient absorption has a distinctly different time and intensity dependence for different tube structures, suggesting a branching to emissive and trap states following photoexcitation. © 2004 American Institute of Physics. [DOI: 10.1063/1.1640339]

## INTRODUCTION

The remarkable electronic properties of single-walled carbon nanotubes (SWNT) indicate a tremendous potential for novel applications.<sup>1</sup> However, spectroscopic access to these exquisite qualities has long been hampered by the strong structural dependence of the electronic density of states<sup>2,3</sup> together with the diversity of diameters and chiral angles of nanotubes as well as aggregation of tubes in all preparations previously available.<sup>4–6</sup> Additionally, the intertube interactions as the result of aggregation mostly wash out any specific spectroscopic features of interest.<sup>7,8</sup> The recent discovery of band-gap fluorescence from a semiconducting SWNT sample rich in individual nanotubes surrounded by cylindrical sodium dodecyl sulfate (SDS) micelles<sup>9</sup> has made it possible to correlate optical spectra with individual tube species as a result of their well-defined optical transitions.<sup>10</sup> The dual wavelength excitation-emission selectivity<sup>10</sup> has also opened a way to experimental study of separate SWNT types. A description of the dynamics following excitation is important to understand the optical properties of SWNT and the characteristic time scales of carrier relaxation, which is essential to many of their potential applications. Here, we

present experimental results from femtosecond fluorescence up-conversion and pump-probe measurements on several distinct nanotube structures.

Figure 1 illustrates schematically the electronic density of states (DOS) of semiconducting SWNT, characterized by sharp van Hove singularities arising from the quasi-one-dimensional nature of nanotubes.<sup>3</sup> The transition energies  $E_{11}$  and  $E_{22}$  are tunable by variation of the nanotube structure<sup>3</sup> and generally correspond to transitions in the near IR and visible spectral regions, respectively.<sup>10</sup> Optical excitation resonant with the second subband at  $E_{22}$  of selected tubes generates an electron ( $e$ ) in the conduction subband  $c_2$  and leaves a hole ( $h$ ) in the valence subband  $v_2$ , respectively. Spatial confinement in the SWNT leads to considerable enhancement in the Coulombic coupling between the photoexcited  $e$  and  $h$  to create strongly bound excitons.<sup>11–13</sup> This is followed by intraband relaxation of the  $e$  and  $h$  ( $c_2 \rightarrow c_1$  and  $v_2 \rightarrow v_1$ ) to the fundamental band gap  $E_{11}$ , where a second subband exciton leads to either one or two first subband excitons or unbound  $e-h$  pairs,<sup>13</sup> depending on the energies of the corresponding transitions and the exciton binding energy.<sup>12</sup> In the present study, the femtosecond time-resolved spontaneous emission and transient absorption are probed at the  $E_{11}$  transitions of selected tubes and thus is sensitive to the relaxation of the excitons and/or  $e-h$  pairs. The carrier

<sup>a)</sup> Author to whom correspondence should be addressed. Electronic mail: GRFleming@lbl.gov

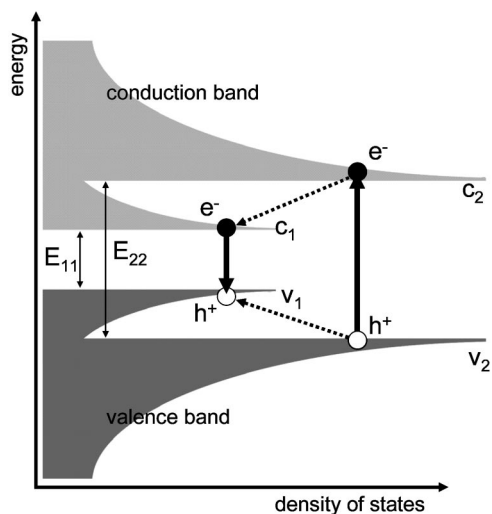


FIG. 1. Schematic density of electronic states for a single nanotube structure. Arrows depict excitation (pump)/emission (probe) wavelengths and interband transitions; dotted arrows represent the intraband electron and hole relaxation processes.

dynamics revealed by transient fluorescence and absorption is determined by the time-dependent product of the  $e$  and  $h$  distributions, and by the sum of these distributions, respectively,<sup>14</sup> and identical dynamics is seen in the two measurements only when  $e$  and  $h$  have identical dynamics.

The strategy in selectively probing the carrier dynamics of a specific tube type is electronically resonant excitation and detection. In practice, this strategy is generally accomplished by varying both the excitation (pump) and emission (probe) wavelengths according to Ref. 10 to ensure electronic resonance with the  $E_{22}$  and  $E_{11}$  transitions of a given nanotube, respectively. A simplification of this general procedure can be further achieved for those tubes with sufficiently close  $E_{22}$  transition energies. Owing to the spectral overlap between their  $E_{22}$  transitions, the use of a single wavelength can simultaneously excite multiple tube structures, and consequently, tube-type selective detection can be realized by simply changing the emission (probe) wavelength. Even though we used ultrashort laser pulses for excitation and detection in our experiment the spectral bandwidth was small enough to ensure selectivity of a specific tube structure.

## EXPERIMENT

Tunable femtosecond excitation pulses (30 fs) with a repetition rate of 250 kHz were generated by an optical parametric amplifier. The excitation beam was focused to a spot size of  $\sim 30$  and  $\sim 75$   $\mu\text{m}$  on the sample in the fluorescence upconversion and transient absorption experiments, respectively. The relative polarization between the excitation and probe (gate) beams was set to  $54.7^\circ$  and the instrument response had a temporal width of about 100 fs (FWHM). Details of the experimental setups are given elsewhere.<sup>15,16</sup> SWNT material was produced by a HiPCO-type generator at Rice University, and the same procedure as described previously was used to prepare a sample rich in individual nanotubes in a surfactant–water system (SDS in  $\text{D}_2\text{O}$ ).<sup>9</sup> In our

experiments, the pathlength of the 1.0 mm sample cell corresponded to a typical optical density of about 0.15. During data acquisition, the samples were circulated using a peristaltic pump in the fluorescence experiment, while in the pump–probe experiment the static sample cell with 1 mm pathlength was continuously translated along the vertical direction. The stability of the sample was checked by recording the absorption spectra before and after the time-resolved measurements.

## RESULTS AND DISCUSSION

In our time-resolved fluorescence experiment, we monitor selected tubes via the following combinations of excitation/emission wavelengths 567/975, 660/950, 660/1119, and 660/1244 nm. These combinations select four tube structures (7,6), (8,3), (6,5), and (9,5), according to Ref. 10. Since the creation of fluorescence photons requires an  $e-h$  recombination, the fluorescence signal is determined by the temporal evolution of the  $e-h$  pair population in  $c_1$ , the lowest conduction band state and in  $v_1$ , the highest valence band state, respectively.<sup>14</sup> Figure 2(a) shows the transient fluorescence intensity at 1244 nm for five different excitation intensities. All transients exhibit the same sharp rise at zero delay time within the time resolution of the instrument, indicating that the intraband  $e$  ( $c_2 \rightarrow c_1$ ) and  $h$  ( $v_1 \rightarrow v_2$ ) relaxations are faster than 100 fs. However, for positive times the fluorescence decays show strong intensity dependence, namely, a faster decay with an increase of excitation intensity. In addition, the overall amplitude of the fluorescence kinetics shows apparently nonlinear dependence on the excitation intensity [Fig. 2(b)]. For the tube structures (8,3), (7,6), and (6,5) exhibiting fluorescence at 950, 975, and 1119 nm, similar behavior is observed (data not shown). One possible explanation for this intensity dependence is an exciton–exciton annihilation process as the result of the simultaneous generation of multiple excitons in a single carbon nanotube.<sup>17</sup> In terms of this model, the kinetic evolution of excitons can be described by

$$\frac{dN(t)}{dt} = -kN(t) - \gamma N(t)^2, \quad (1)$$

where  $N(t)$  is the mean number of excitons created in the first subband of a selected tube structure,  $k$  the linear exciton decay rate, and  $\gamma$  the rate of biexciton annihilation. An analytical solution of Eq. (1) is readily obtained and for the short-time kinetics, where  $kt < 1$ , this solution further simplifies to<sup>18</sup>

$$N(t) = \frac{N(0)}{1 + N(0)\gamma \cdot t}, \quad (2)$$

where  $N(0)$  is the initial number of excitons. As the fluorescence intensity,  $I(t)$ , is proportional to  $N(t)$ , a linear time dependence of the inverse of the normalized fluorescence intensity,  $I(t)/I_0$ , is obtained:

$$\left(\frac{I(t)}{I_0}\right)^{-1} \sim \left(\frac{N(t)}{N(0)}\right)^{-1} = \gamma N(0) \cdot t + 1, \quad (3)$$

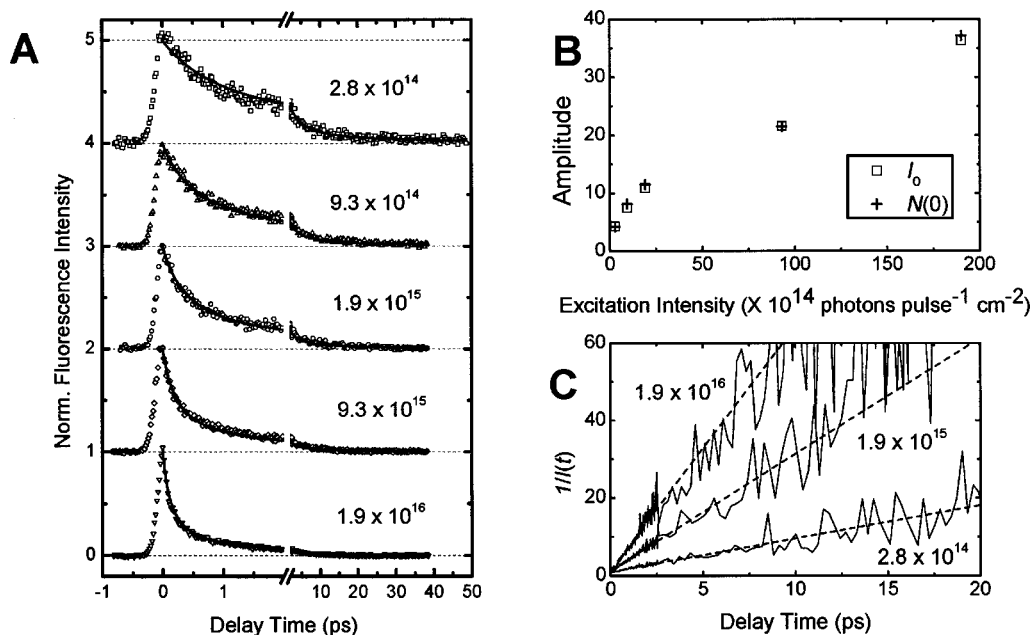


FIG. 2. (a) Normalized time-resolved fluorescence intensity for the (9,5) tube structure at different excitation intensities. The solid lines represent the global fits according to Eq. (2). (b) Plot of the maximum fluorescence intensities  $I_0$  and the fitted parameter  $N(0)$  vs the excitation intensities. (c) The same data as in (a) plotted as the inverse of intensity over time.

where  $I(t)$  is the fluorescence intensity at time  $t$  and  $I_0$  the maximum fluorescence intensity. Plotting the inverse of the normalized fluorescence kinetics shown in Fig. 2(a) as a function of time results in a linear behavior for delay times up to  $\sim 10$  ps [Fig. 2(c)]. This suggests that exciton annihilation dominates the dynamics in this time range, even for the lowest excitation intensity ( $3 \times 10^{14}$  photons/pulse  $\text{cm}^{-2}$ ) and the assumption of  $kt < 1$  is justified.

Detailed analyses of the fluorescence kinetics measured over the full scan range ( $\sim 40$ – $50$  ps) were performed using Eq. (2) globally, where  $\gamma$  and  $N(0)$  were taken as global and local fitting parameters, respectively. As shown in Fig. 2(a), the various fluorescence kinetics can be well described by Eq. (2) and only a minor deviation is seen in the kinetics detected at higher excitation intensity at a delay time of  $\sim 5$  ps. This global analysis gives  $\gamma = 0.19 \text{ ps}^{-1}$  and  $N(0) = 4.2, 8.1, 11.5, 21.5,$  and  $37.2$  for the five excitation intensities used. In addition, the values of  $N(0)$  obtained are plotted in Fig. 2(b) versus excitation intensity, which shows a nearly identical dependence to that of the maximum fluorescence intensity. All these fitting parameters are relative numbers, which are inversely (for  $\gamma$ ) or linearly [for  $N(0)$ ] proportional to the amplitudes of the fluorescence signals. To obtain absolute values for these parameters, one needs to independently determine the mean number of the first subband excitons created in a given tube type at different excitation intensities. This determination requires an accurate absorption cross section per tube and the branching ratio (to form first subband exciton and unbound  $e-h$  pairs) following the intraband relaxation. Both the cross section and branching ratio are currently unavailable. Nevertheless, the similar dependence of  $N(0)$  and  $I_0$  on excitation intensity [Fig. 2(b)] shows the self-consistency of the analysis outlined above.

From a microscopic point of view, exciton annihilation

occurs when two excitons approach each other within the so-called reaction radius ( $R_c$ ), at which two excitons will annihilate immediately.<sup>18</sup> At low excitation intensity, the spatial separation between excitons increases to  $> R_c$ , and annihilation will require exciton motion.<sup>18</sup> Such motion will be mediated by Coulombic interactions and since the  $E_{11}$  transitions are narrow and have small Stokes shifts,<sup>9</sup> the Franck-Condon factors will be large and energy migration rapid.

The analysis outlined above implicitly assumes that the dimensionality of exciton diffusion is  $\geq 2$ .<sup>18</sup> To examine this assumption, we plotted the inverse of the normalized fluorescence intensity  $I(t)/I_0$  versus  $t^{1/2}$ , which should give rise to a straight line for strictly one-dimensional diffusional exciton motion.<sup>18</sup> As shown in Fig. 3, the plot for the kinetics of the (9,5) tube structure, measured at 1244 nm under the

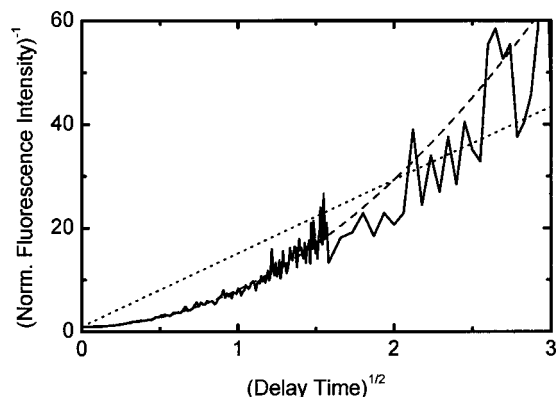
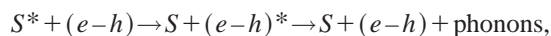


FIG. 3. Plots of  $[I(t)/I_0]^{-1}$  vs  $\sqrt{t}$  for the fluorescence kinetics of the (9,5) tube structure for the highest excitation intensity. The calculated results, obtained by assuming a dimensionality of exciton motion being 1 (dotted line) and  $\geq 2$  (dashed line), are also shown (see the text).

highest excitation intensity, shows a clear deviation from a straight line. For a qualitative analysis of the dimensionality, we further calculated the inverse of the normalized fluorescence intensity using the values for  $\gamma$  and  $N(0)$  obtained above, assuming that the dimensionality  $d$  is either 1 or  $\geq 2$ , respectively, and the time-independent annihilation rate in the 1-D case has the same numerical value as  $\gamma$  (in  $\text{ps}^{-1/2}$ ). A plot of the calculated data versus  $t^{1/2}$  shows a straight line for  $d=1$ , whereas for  $d \geq 2$ , it bends upward. As shown in Fig. 3, the experimental curve measured at 1244 nm closely resembles the case for  $d \geq 2$ . This greater than unity dimensionality of exciton motion seems to be intuitively in contradiction to the one-dimensional structure of ideal nanotubes. Such exciton motion may be possible if the physical size of the exciton is smaller than the diameter of the tube and motion of the exciton occurs on the surface of the nanotubes. Recent theoretical calculations show that the exciton Bohr radius is larger than the tube diameter.<sup>12,19</sup> For example, Spataru *et al.*<sup>19</sup> find that the extent of the excitons in the (8,0) tube is almost 25 Å. We need to emphasize that our analysis is based on the assumption of purely diffusive exciton motion. If the exciton motion is ballistic, as is observed in the conduction of nanotubes,<sup>20</sup> the approach used is inappropriate and the value of  $d$  may not have a simple physical meaning. Clearly further study, including electronic structure calculations of the specific tubes we have studied, is required to clarify this point.

Exciton annihilation does appear to provide an adequate explanation of the excitation intensity dependence of the fluorescence decays and additionally may provide insight into the microscopic motion of excitons in SWNT. However, the dimensionality issue suggests we consider an alternative explanation for the experimental observations. Since a substantial amount of unbound  $e-h$  pairs form following the intraband relaxation, diffusion of these  $e-h$  pairs in the SWNT<sup>21</sup> will result in collisions with excitons, leading to a quenching of excitons. Exciton ionization occurs because the rapid intraband relaxation leads to the formation of first sub-band excitons with a total kinetic energy comparable to or even larger than the exciton binding energy ( $E_b$ ).<sup>21</sup> Considering the (9,5) tube as an example, the kinetic energy given by  $E_{22} - E_{11}$  is about  $6860 \text{ cm}^{-1}$ , while the calculated  $E_b$  for a tube with similar diameter is only  $3230 \text{ cm}^{-1}$ .<sup>12</sup> A quenching phenomenon of this type was observed previously in conjugated polymers,<sup>22</sup> and can be described by



where  $S$  represents the exciton and  $*$  stands for an excited species. Neglecting the reformation of excitons from unbound  $e-h$  pairs, the dynamics of this quenching process can be described by the following rate equations:

$$\begin{aligned} \frac{dN(t)}{dt} &= -k_1 N(t) - k_2 N_{eh}(t) N(t), \\ \frac{dN_{eh}(t)}{dt} &= -k_3 N_{eh}(t), \end{aligned} \quad (4)$$

where  $N(t)$  and  $N_{eh}(t)$  are the densities of excitons and unbound ( $e-h$ ) pairs, respectively,  $k_1$  and  $k_3$  are their corre-

sponding intrinsic decay rates, and  $k_2$  is the constant of exciton quenching by the unbound ( $e-h$ ) pair. Using initial conditions of  $N(0)=a$  and  $N_{eh}(0)=1-a$ , analytical solutions of Eqs. (4) are straightforward to obtain. We modeled the time dependence of  $N(t)$  by taking  $k_1$ ,  $k_2$ ,  $k_3$ ,  $a$ , and an amplitude scaling factor as free parameters, reasonable fits to experimental data, especially at lower excitation intensities, can be obtained (data not shown). However, the parameters obtained from the modeling lead to an unrealistically high percentage of exciton ionization, up to  $\sim 98\%$ , which suggest that this mechanism must be of minor importance in our case.

To obtain a different point of view on the carrier dynamics we also studied the transient absorption of SWNT, which is sensitive to the  $e$  and  $h$  distributions independently.<sup>14</sup> In this pump-probe experiment, we selected five tube structures, namely the (6,4), (9,1), (6,5), (8,3), and (7,5) structures, by choosing appropriate pump/probe wavelength combinations, peaking at 581/873, 693/912, 567/975, 660/952, and 660/1023 nm, respectively.<sup>10</sup> The pump-probe kinetics measured at different wavelengths are generally independent of pump intensity ( $J$ ) for  $J \leq 2 \times 10^{15}$  photons/pulse  $\text{cm}^2$ . This threshold required to obtain intensity-dependent kinetics in the pump-probe experiment is approximately one order of magnitude higher than the lowest excitation intensity used in the fluorescence up-conversion measurements. Figures 4(a) and 4(b) compare the normalized time-resolved fluorescence decays of (6,5) tubes with the corresponding decays of the pump-induced transmission at the fundamental band gap. The increased transmission in the pump-probe kinetics is caused by a bleach due to the occupation of holes in the  $\nu_1$  state as well as by stimulated emission from electrons in the  $c_1$  state. The same trends are observed in both experiments, namely a faster decay for higher excitation densities. In contrast, the pump-probe traces probed at 1024 nm for the (7,5) tube structure exhibit the opposite trend: The induced transmission decay in the first picosecond slows down with an increase of excitation density and the change of the kinetics persists to an extremely low pump intensity ( $2 \times 10^{14}$  photons/pulse  $\text{cm}^2$ ) compared with the results obtained at other pump/probe wavelengths. Furthermore, a long-lived induced absorption observed at lower pump intensity vanishes at higher pump intensities. This distinctly different decay behavior at 975 and 1023 nm with the change of pump intensity indicates the existence of some so far undefined charge trap states, which persist after the relaxation of excitons.<sup>23</sup> The noticeable difference in the thresholds for intensity-dependent kinetics in the pump-probe and fluorescence experiments, together with the opposite trend with the increase of pump intensity at 975 and 1023 nm [see Figs. 4(b) and 4(c)] suggests that the transient species contributing to the pump-probe signal is different to that dominating the time-resolved fluorescence. Recombination of unbound  $e-h$  pairs may lead to photon emission, however, this emission is expected to be spectrally distinct from the radiative relaxation of excitons, owing to the large  $E_b$  as the result of spatial confinement.<sup>12</sup> However, the unbound  $e$  and  $h$  will contribute individually to the pump-probe signals.<sup>14</sup> In fact, a contribution from unbound electrons in SWNT has been ob-

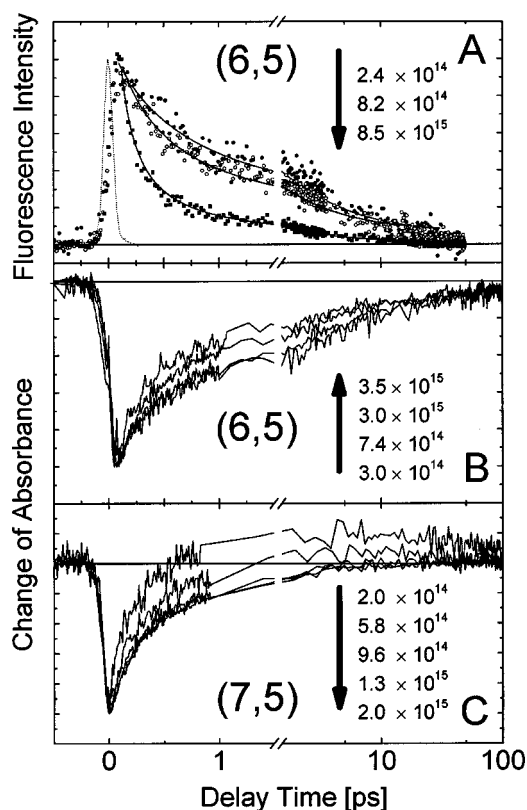


FIG. 4. (a) Time-resolved fluorescence kinetics probed for the (6,5) tube structure at different excitation intensities. The solid lines represent the global fits according to Eq. (2) and the dotted line is the instrumental response. (b) Transient induced transmission of the same tube structure (6,5) measured at different pump intensities. Note that indistinguishable decays were found at the two lowest intensities. (c) Pump-probe kinetics detected for the tube structure (7,5) under different pump intensities, and remarkable kinetic changes were observed at lower pump intensities.

served in a previous pump-probe experiment.<sup>24</sup> The relatively high threshold required to obtain pump intensity-dependent kinetics supports the attribution of an additional contribution to the pump-probe signal from unbound  $e-h$ . It was reported previously that variation of the pump intensity has little effect on the recombination (radiative and non-radiative) dynamics of unbound  $e-h$  pairs in conjugated polymers.<sup>25</sup> On the other hand, the opposite decay trend with the increase of pump intensity observed at 975 and 1023 nm [see Figs. 4(b) and 4(c)], which suggests the involvement of additional electronic transition(s), probably from charge trap states or even triplet states. The additional transition(s) must have a different dependence on the pump intensity in comparison to the transitions at the band gap.

The distinctly different behavior shown in Figs. 4(b) and 4(c) represents two extreme cases. The data obtained for the tube structures (9,1) and (6,4) show induced absorption as observed for the (7,5) tube at the lowest pump intensity, but with much smaller amplitudes and more rapid decay within a few picoseconds, whereas the (8,3) tube structure behaves in a similar manner to the (6,5) tube (data not shown). In addition to the distinct difference in the overall decay profiles, all the pump intensity-independent kinetics are found to exhibit nonexponential decay, which is indicative of a diffusional motion of excitons in the presence of static quenching

sites.<sup>26,27</sup> These quenching sites may be formed by chemical impurities and/or structural defects in the SWNT, and their presence has been found to substantially alter the DOS.<sup>28</sup> Furthermore, substantial variation of the tube length in the preparation may also contribute to the observed nonexponential decay. A detailed analysis of this nonexponential decay using SWNT preparations with well-characterized defects/impurities will enable an exploration of the separate effects of the static heterogeneity and the quenching of excitons.

## CONCLUDING REMARKS

In summary, the combination of ultrafast fluorescence and absorption spectroscopy provides a new point of view into the optical properties of SWNT. The striking difference between the two types of measurement points to a branching of carrier relaxation pathways as well as the influence of trapped states. Recent *ab initio* many-electron Green's function calculations of the electronic structure of the (8,0) semiconducting SWNT show that excitonic effects dramatically alter the optical properties and Fig. 1 provides, at best, only a crude caricature of the tube electronic structure. Attempts to optimize emission yields, for example, will be greatly aided by an understanding of the factors contributing to the branching driving the carrier relaxation. As a next step we will carry out spectrally resolved pump-probe spectroscopy, which has the potential to allow a separate observation of the trapped states due to their spectral shift. Also, a direct excitation of selected  $E_{11}$  transitions will greatly simplify the kinetics and help identify different relaxation mechanisms and the states involved.

## ACKNOWLEDGMENTS

The research at Berkeley has been supported by the National Science Foundation. J.S. thanks the German Academic Exchange Service (DAAD) for support. We thank D. S. Chemla, S. G. Louie, S. Ismail-Beigi, C. D. Spataru, and S. L. Dexheimer for a helpful discussion.

- <sup>1</sup>R. H. Baughman, A. A. Zakhidov, and W. A. de Heer, *Science* **297**, 787 (2002).
- <sup>2</sup>S. Saito, G. Dresselhaus, and M. S. Dresselhaus, *Physical Properties of Carbon Nanotubes* (Imperial College Press, London, 1998).
- <sup>3</sup>T. W. Odom, J.-L. Huang, P. Kim, and C. M. Lieber, *J. Phys. Chem. B* **104**, 2794 (2000).
- <sup>4</sup>A. Thess, R. Lee, P. Nikolaev *et al.*, *Science* **273**, 483 (1996).
- <sup>5</sup>S. Bandow, A. M. Rao, K. A. Williams, A. Thess, R. E. Smalley, and P. C. Eklund, *J. Phys. Chem. B* **101**, 8839 (1997).
- <sup>6</sup>R. Bandyopadhyaya, E. Nativ-Roth, O. Regev, and R. Yerushalmi-Rozen, *Nano Lett.* **2**, 25 (2002).
- <sup>7</sup>Y.-K. Kwon, S. Saito, and D. Tomaneck, *Phys. Rev. B* **58**, R13314 (1998).
- <sup>8</sup>M. Ouyang, J.-L. Huang, C. L. Cheung, and C. M. Lieber, *Science* **292**, 702 (2001).
- <sup>9</sup>M. J. O'Connell, S. M. Bachilo, C. B. Huffman *et al.*, *Science* **297**, 593 (2002).
- <sup>10</sup>S. M. Bachilo, M. S. Strano, C. Kittrell, R. H. Hauge, R. E. Smalley, and R. B. Weisman, *Science* **298**, 2361 (2002).
- <sup>11</sup>T. Ando, *J. Phys. Soc. Jpn.* **66**, 1066 (1997).
- <sup>12</sup>T. G. Pedersen, *Phys. Rev. B* **67**, 073401 (2003).
- <sup>13</sup>C. L. Kane and E. J. Mele, *Phys. Rev. Lett.* **90**, 207401 (2003).

- <sup>14</sup>J. Shah, *Ultrafast Spectroscopy of Semiconductors and Semiconductor Nanostructures*, 2nd ed. (Springer-Verlag, Berlin, 1999).
- <sup>15</sup>P. J. Walla, J. Yom, B. P. Krueger, and G. R. Fleming, *J. Phys. Chem. B* **104**, 4799 (2000).
- <sup>16</sup>Y.-Z. Ma, N. E. Holt, X.-P. Li, K. K. Niyogi, and G. R. Fleming, *Proc. Natl. Acad. Sci. U.S.A.* **100**, 4377 (2003).
- <sup>17</sup>L. Valkunas, G. Trinkunas, V. Liuolia, and R. van Grondelle, *Biophys. J.* **69**, 1117 (1995).
- <sup>18</sup>H. van Amerongen, L. Valkunas, and R. van Grondelle, *Photosynthetic Excitons* (World Scientific, Singapore, 2000).
- <sup>19</sup>C. D. Spataru, S. Ismail-Beigi, L. X. Benedict, and S. G. Louie, *Phys. Rev. Lett.* (in press).
- <sup>20</sup>S. Frank, P. Poncharal, Z. L. Wang, and W. A. de Heer, *Science* **280**, 1744 (1998).
- <sup>21</sup>M. Freitag, Y. Martin, J. A. Misewich, R. Martel, and P. Avouris, *Nano Lett.* **3**, 1067 (2003).
- <sup>22</sup>Y. V. Romanovskii, V. I. Arkhipov, and H. Bassler, *Phys. Rev. B* **64**, 033104 (2001).
- <sup>23</sup>M. C. Brelle, J. Z. Zhang, L. Nguyen, and R. K. Mehra, *J. Phys. Chem. A* **103**, 10194 (1999).
- <sup>24</sup>J.-S. Lauret, C. Voisin, G. Cassabois, C. Delalande, P. Roussignol, O. Jost, and L. Capes, *Phys. Rev. Lett.* **90**, 057404 (2003).
- <sup>25</sup>M. Yan, L. J. Rothberg, F. Papadimitrakopoulos, M. E. Galvin, and T. M. Miller, *Phys. Rev. Lett.* **72**, 1104 (1994).
- <sup>26</sup>B. Y. Balagurov and V. G. Valks, *Sov. Phys. JETP* **38**, 968 (1974).
- <sup>27</sup>M. Yan, L. J. Rothberg, F. Papadimitrakopoulos, M. E. Galvin, and T. M. Miller, *Phys. Rev. Lett.* **73**, 744 (1994).
- <sup>28</sup>J.-C. Charlier, *Acc. Chem. Res.* **35**, 1063 (2002).